

Valence bond order in a honeycomb antiferromagnet coupled to quantum phonons

Manuel Weber 

Department of Physics, Georgetown University, Washington, DC 20057, USA



(Received 13 October 2020; accepted 11 December 2020; published 11 January 2021)

We use exact quantum Monte Carlo simulations to demonstrate that the Néel ground state of an antiferromagnetic $SU(2)$ spin- $\frac{1}{2}$ Heisenberg model on the honeycomb lattice can be destroyed by a coupling to quantum phonons. We find a clear first-order transition to a valence bond solid state with Kekulé order instead of a deconfined quantum critical point. However, quantum lattice fluctuations can drive the transition towards weakly first order, revealing a tunability of the transition by the retardation of the interaction. In contrast to the one-dimensional case, our phase diagram in the adiabatic regime is qualitatively different from the frustrated J_1 - J_2 model. Our results suggest that a coupling to bond phonons can induce Kekulé order in Dirac systems.

DOI: [10.1103/PhysRevB.103.L041105](https://doi.org/10.1103/PhysRevB.103.L041105)

Exotic phases and phase transitions in quantum many-particle systems have attracted a lot of interest in the last few years. A recent focus has been on valence bond solid (VBS) phases in two-dimensional (2D) spin- $\frac{1}{2}$ antiferromagnets (AFMs) where translational symmetry is spontaneously broken via the formation of dimers between neighboring spins [1]. The proliferation of topological defects in the AFM/VBS order parameter [2–4] has been proposed to drive a continuous quantum phase transition between the two phases. The scenario of a deconfined quantum critical point (DQCP) [5,6] is beyond the Landau-Ginzburg-Wilson paradigm in which competing orders with different broken symmetries require a first-order transition. Furthermore, the interplay between the topological defects of the VBS phase and disorder is currently being explored [7].

VBS order often appears in frustrated spin models, but their numerical study in 2D is usually restricted to small system sizes or approximate schemes. Large-scale quantum Monte Carlo (QMC) simulations give exact results for a class of sign-problem-free Hamiltonians called J - Q models [8] that are specifically designed to generate the desired orders. While J - Q models show strong evidence of a continuous AFM-VBS transition—most notably on the square lattice [8–10]—the scenario of a weak first-order transition cannot be completely ruled out [11,12]. Recently, unconventional first-order transitions with enhanced symmetry were reported [13]. It is of current interest to find VBS phases also in more realistic models beyond designer Hamiltonians.

In quasi-one-dimensional systems such as the organic TTF compounds [14] and the inorganic material CuGeO_3 [15], VBS order often arises from the spin-Peierls instability [16,17], which is closely related to a $2k_F$ Fermi-surface instability in electronic models. A one-dimensional (1D) Heisenberg model is unstable towards dimerization for any finite coupling to classical phonons because the gain in magnetic energy is higher than the loss in elastic energy. However, quantum lattice fluctuations can stabilize a gapless phase with critical AFM correlations below a critical coupling. The phase diagrams of 1D spin-phonon models have been

determined numerically [18–27]. For high phonon frequencies, the spin-Peierls problem maps to the frustrated J_1 - J_2 model with next-nearest-neighbor Heisenberg exchange [28–31]. In particular, the quantum phase transition at finite phonon frequencies is in the same universality class as in the J_1 - J_2 model [27].

The relevance of spin-phonon interactions in 1D is acknowledged by the fact that—even in other contexts—the VBS state is sometimes called the *spin-Peierls state* [2,3,32]. By contrast, the nature and even the existence of VBS order in 2D is still under debate and has been explored only on the square lattice. The spin-Peierls model was initially studied in the context of high- T_c superconductivity as the large- U limit of the Peierls-Hubbard model. Different dimerization patterns were discussed as the ground-state configurations of classical phonons [33–39], even a resonating valence bond state was proposed [40,41]. The stability of the spin-Peierls state was questioned because a large Hubbard repulsion favors AFM order and suppresses VBS order in 2D [42]. So far, exact numerical simulations have been inhibited by the large bosonic Hilbert space and difficult phonon sampling. The only available QMC study which approached the full quantum-phonon problem did not find VBS order [43].

The honeycomb lattice has a lower coordination number than the square lattice, which makes the VBS state energetically more favorable. A columnar VBS state with Kekulé order (see the inset of Fig. 1) was found in a J - Q model, and its AFM-VBS transition was interpreted in terms of a DQCP [44–47]. Similar transitions appear in Dirac systems [48,49], where the emergence of Kekulé order has been a recent focus of theoretical [50–58] and experimental [59,60] studies. Interaction effects in graphene have attracted additional interest since the discovery of superconductivity in twisted bilayer graphene [61].

In this Letter, we demonstrate that spin-phonon coupling can stabilize a columnar VBS state and determine the ground-state phase diagram of the spin-Peierls model as a function of phonon frequency (see Fig. 1). Our simulations were made possible by a recently developed QMC method that solves

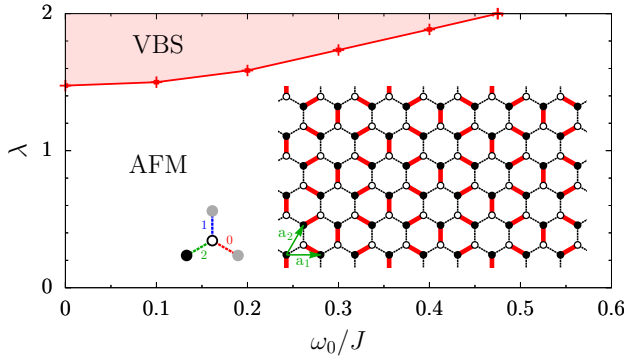


FIG. 1. Phase diagram of the spin-Peierls model (1) as a function of phonon frequency and spin-phonon coupling from QMC simulations. The large inset shows a honeycomb lattice with columnar VBS order where strong (weak) links represent a high (low) $\langle \hat{\Pi}_{ij} \rangle$. The small inset depicts the two sites, A, B , and the three bonds, $\mu = 0, 1, 2$, that belong to a unit cell.

the full quantum-phonon problem efficiently using retarded interactions [62]. The AFM-VBS transition is strongly first order for classical phonons, but quantum lattice fluctuations can drive the transition towards weakly first order. We discuss how our results are related to the putative DQCP scenario on the honeycomb lattice. Furthermore, we debate whether retardation effects can induce the physics of the frustrated J_1 - J_2 model at high phonon frequencies which are not accessible to our simulations. At low frequencies, the two models show different orders, unlike in the 1D case. Finally, our results suggest that a coupling to bond phonons can induce Kekulé order in Dirac systems.

Model and method. We consider the spin-Peierls model

$$\hat{H} = \sum_{\langle i,j \rangle} (J + \alpha \hat{Q}_{ij}) \hat{\mathbf{S}}_i \cdot \hat{\mathbf{S}}_j + \sum_{\langle i,j \rangle} \left(\frac{1}{2M} \hat{P}_{ij}^2 + \frac{K}{2} \hat{Q}_{ij}^2 \right), \quad (1)$$

where the antiferromagnetic exchange J is modulated via a coupling α to optical bond phonons with frequency $\omega_0 = \sqrt{K/M}$. The spin- $\frac{1}{2}$ operators $\hat{\mathbf{S}}_i$ are defined on the sites i of a honeycomb lattice, whereas the phonon momenta \hat{P}_{ij} and displacements \hat{Q}_{ij} act on the links between nearest neighbors $\langle i, j \rangle$. In the following, we use $J = 1$ as the unit of energy, define the dimensionless coupling $\lambda = \alpha^2 / (2KJ)$, and set $\hbar, k_B = 1$.

The phonons can be integrated out exactly using the imaginary-time path integral. The partition function becomes $Z = Z_0 \text{Tr} \hat{\mathcal{T}}_\tau e^{-\hat{\mathcal{H}}}$, with $\hat{\mathcal{H}} = \hat{\mathcal{H}}_J + \hat{\mathcal{H}}_\lambda$ and

$$\hat{\mathcal{H}}_J = -J' \int_0^\beta d\tau \sum_{\langle i,j \rangle} \hat{\Pi}_{ij}(\tau), \quad J' = J \left(1 - \frac{\lambda}{2} \right), \quad (2)$$

$$\hat{\mathcal{H}}_\lambda = -\lambda J \iint_0^\beta d\tau d\tau' \sum_{\langle i,j \rangle} \hat{\Pi}_{ij}(\tau) P(\tau - \tau') \hat{\Pi}_{ij}(\tau'). \quad (3)$$

The spin-phonon coupling leads to a retarded interaction $\hat{\mathcal{H}}_\lambda$ between singlet projectors $\hat{\Pi}_{ij} = \frac{1}{4} - \hat{\mathbf{S}}_i \cdot \hat{\mathbf{S}}_j$ at different times τ, τ' and is mediated by the free-phonon propagator $P(\tau) = e^{-\omega_0 \tau} \omega_0 / (1 - e^{-\omega_0 \beta})$. Because $\hat{\mathbf{S}}_i \cdot \hat{\mathbf{S}}_j$ is shifted by $\frac{1}{4}$, the Heisenberg exchange J' gets renormalized with λ . Here,

$\beta = 1/T$ is the inverse temperature, and Z_0 includes the partition function of free phonons.

For our simulations we used a recently developed QMC method for retarded interactions [62] that is based on a diagrammatic expansion of Z/Z_0 in $\hat{\mathcal{H}}$. The method is closely related to the stochastic series expansion [63] and makes use of efficient directed-loop updates [64]. It has only statistical errors and is free of a sign problem for $\lambda \leq 2$ ($J' \geq 0$). The use of retarded interactions avoids the difficulties of direct phonon sampling which inhibited previous studies of the 2D case, but system sizes are still limited by the generically difficult sampling near a first-order transition. We use an exchange Monte Carlo method [65,66] to improve simulations in the VBS phase. Phonon observables can be recovered from the perturbation expansion using generating functionals [67]. Further details on our method are presented elsewhere [68].

Simulations were performed on $L \times L$ honeycomb lattices with $2L^2$ spins and periodic boundary conditions. We used $\beta J = 2L$, which is suitable for detecting the ground-state order of a continuous phase transition with dynamical exponent $z = 1$ or a first-order transition.

Results. The phase diagram in Fig. 1 contains AFM and VBS phases which can be identified from a finite-size analysis of the (basis-dependent) order parameters [47]

$$\hat{\Psi}_{\text{AFM}}(\mathbf{q}) = \frac{1}{2L^2} \sum_{\mathbf{r}} (\hat{\mathbf{S}}_{\mathbf{r}A} - \hat{\mathbf{S}}_{\mathbf{r}B}) e^{i\mathbf{q} \cdot \mathbf{r}}, \quad (4)$$

$$\hat{\Psi}_{\text{VBS}}(\mathbf{q}) = \frac{1}{2L^2} \sum_{\mathbf{r}} \sum_{\mu=0}^2 \hat{\Pi}_{\mathbf{r}\mu} e^{2\pi i \mu / 3} e^{i\mathbf{q} \cdot \mathbf{r}}. \quad (5)$$

Here, \mathbf{r} is the position vector of the Bravais lattice. Each unit cell has two sites, A, B , and three bonds, $\mu = 0, 1, 2$, which are chosen as depicted in Fig. 1. AFM order breaks the $SU(2)$ spin symmetry and appears at $\mathbf{Q}_{\text{AFM}} = (0, 0)$, whereas the columnar VBS state breaks Z_3 lattice symmetry such that spin singlets are arranged in a Kekulé pattern with $\mathbf{Q}_{\text{VBS}} = (2\pi/3, -2\pi/3)$, as shown in Fig. 1. We measure $C_\alpha(\mathbf{q}) = \langle |\hat{\Psi}_\alpha^z(\mathbf{q})|^2 \rangle$ after replacing $\hat{\mathbf{S}}_i \rightarrow \hat{\mathbf{S}}_i^z$ in Eqs. (4) and (5) to calculate the correlation ratios [69]

$$R_\alpha = 1 - \frac{C_\alpha(\mathbf{Q}_\alpha + \delta\mathbf{q})}{C_\alpha(\mathbf{Q}_\alpha)}, \quad (6)$$

with $\delta\mathbf{q} = (0, 2\pi/L)$. When $L \rightarrow \infty$, $R_\alpha(L) \rightarrow 1$ in the corresponding ordered phase, and $R_\alpha(L) \rightarrow 0$ in the disordered phase. The same holds for the Binder cumulant $U_{\text{VBS}} = 2 - \langle |\hat{\Psi}_{\text{VBS}}^z(\mathbf{Q}_{\text{VBS}})|^4 \rangle / \langle |\hat{\Psi}_{\text{VBS}}^z(\mathbf{Q}_{\text{VBS}})|^2 \rangle^2$.

Figure 2 shows our results for the retardation-driven AFM-VBS transition at $\lambda = 2$ [70]. Both orders can be identified from the correlation ratios in Fig. 2(a), which indicate a sharp transition at $\omega_{0,c}/J \approx 0.47$. The Binder ratio in Fig. 2(b) develops a negative peak that diverges with L —a typical finite-size effect at a first-order transition and a result of phase coexistence separated by an energy barrier [71]. Further evidence is given by an emerging discontinuity in the free-energy derivative $dF/d\omega_0$ in Fig. 2(c). Precise extrapolation of $\omega_{0,c}$ is complicated by the nonmonotonic drift of finite-size estimates towards lower (higher) ω_0 for $L < 24$ ($L > 24$) as well as difficult Monte Carlo sampling in the coexistence region.

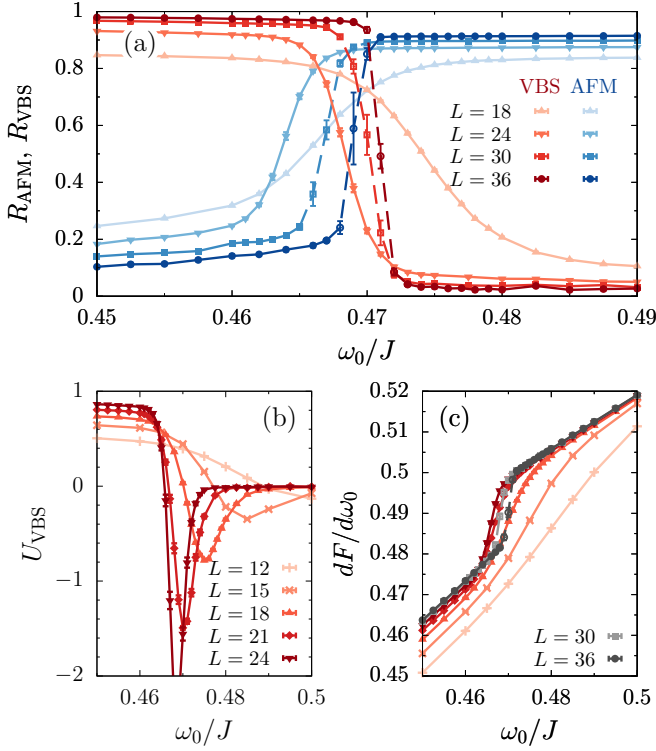


FIG. 2. Finite-size analysis of the AFM-VBS transition at $\lambda = 2$ as a function of ω_0 . (a) AFM/VBS correlation ratios, (b) VBS Binder ratio, and (c) free-energy derivative $dF/d\omega_0$. Labels in (b) also apply to (c). Open symbols and dashed lines represent data points where the tunneling times between coexisting orders are longer than our simulation times.

The nature of the VBS phase is not entirely determined by its ordering vector. Besides the columnar VBS state illustrated in Fig. 1, $\mathbf{Q}_{\text{VBS}} = (2\pi/3, -2\pi/3)$ can also correspond to a plaquette VBS state where strong and weak links are interchanged. The two states are distinguished by the phase of the complex VBS order parameters [47]. We consider the modified field $\hat{\Psi}'_{\text{VBS}}$ by replacing $\hat{\Pi}_{r\mu} \rightarrow (J + \alpha \hat{Q}_{r\mu})\hat{\Pi}_{r\mu}$ in Eq. (5) because its expectation value $\Psi'_{\text{VBS}} = (2L^2\beta)^{-1} \sum_{r\mu} \langle n(\hat{\Pi}_{r\mu}) \rangle_{\text{MC}} e^{2\pi i\mu/3} e^{i\mathbf{Q}_{\text{VBS}} \cdot \mathbf{r}}$ can be easily estimated from the number of $\hat{\Pi}_{r\mu}$ per Monte Carlo configuration [8,67]. The histogram of Ψ'_{VBS} in Fig. 3(a) illustrates that VBS order appears at the columnar angles

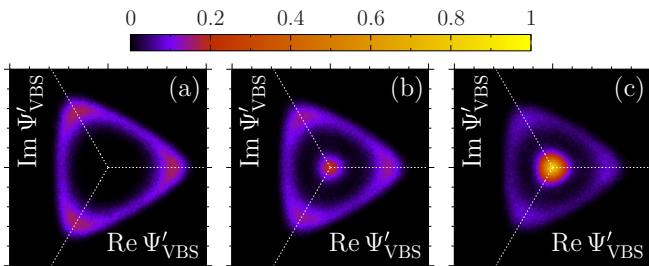


FIG. 3. Histograms of the VBS order parameter Ψ'_{VBS} across the AFM-VBS transition for (a) $\omega_0/J = 0.45$, (b) $\omega_0/J = 0.466$, and (c) $\omega_0/J = 0.47$. Here, $L = 18$ and $\lambda = 2$.

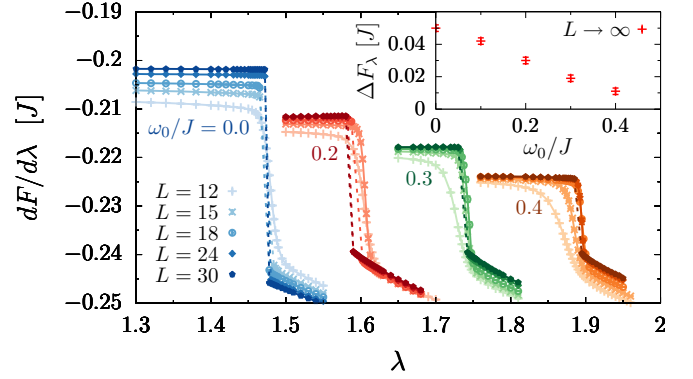


FIG. 4. Free-energy derivative as a function of λ for different ω_0 and L . The inset shows the jump at the critical coupling extrapolated to $L \rightarrow \infty$. The color scheme is based on Ref. [72].

$e^{2\pi i\mu/3}$. The emergence of a central peak in Figs. 3(b) and 3(c) indicates coexisting AFM order. Moreover, the threefold anisotropy of the VBS order parameter remains robust in the coexistence region.

Figure 4 shows the free-energy derivative $dF/d\lambda$ for different ω_0 . The critical couplings in Fig. 1 are determined from the discontinuities in $dF/d\lambda$ and increase with increasing ω_0 . The strength of a first-order transition can be characterized by the size of the jump in its free-energy derivative. To estimate $\Delta F_\lambda(L)$, we extrapolate the two branches of $dF/d\lambda$ towards the center of the coexistence region. A final extrapolation $L \rightarrow \infty$ leads to the jumps summarized in the inset of Fig. 4. We find that the transition is significantly weakened with increasing ω_0 .

Discussion. The nature of the AFM to columnar VBS transition on the honeycomb lattice has been studied numerically in the J - Q model [44–47]. A finite-size analysis obtained critical exponents with logarithmic violations of scaling, consistent with the interpretation of a continuous transition on the square lattice [10]. However, instead of showing an emergent U(1) symmetry at criticality [5], as observed on the square lattice [8], $\hat{\Psi}_{\text{VBS}}(\mathbf{Q}_{\text{VBS}})$ retained a threefold anisotropy which was interpreted in terms of near-marginal behavior of the topological defects [44]. Conformal bootstrap as well as an analysis of anomalies in corresponding field theories suggested that threefold monopoles are slightly relevant at criticality in SU(2) spin models on the honeycomb lattice [73–75] but that lattice sizes of $L \leq 72$ [44] and $L \leq 96$ [46] were too small to find evidence of a weak first-order transition in the J - Q model. The spin-Peierls model studied in this Letter serves as an example where the AFM-VBS transition is clearly first order already on small system sizes and therefore follows the Landau-Ginzburg-Wilson paradigm. The different length scales seem to originate from the retarded nature of $\hat{\mathcal{H}}_\lambda$. The first-order transition is strongest at $\omega_0 = 0$, where the nontrivial minimization of $\langle \hat{H}(Q_{ij}) \rangle$ in terms of the real-valued static displacements permits only certain ordering patterns [76]. Here, the interaction range in time, $P(\tau) \sim e^{-\omega_0\tau}$, is largest, but the transition is significantly weakened with increasing ω_0 . In J - Q models, singlet projectors $\hat{\Pi}_{ij}$ interact at equal times but between different bonds of the lattice to induce VBS order.

Our numerical study is restricted to $\lambda \leq 2$ due to a sign problem, but it is worth speculating on how the phase diagram in Fig. 1 continues for $\omega_0/J > 0.5$. We expect that ω_0 tunes the AFM-VBS transition towards weakly first order, as the discontinuity of $dF/d\lambda$ in Fig. 4 tends to further decrease. A reliable extrapolation of $\Delta F_\lambda(\omega_0)$ is out of reach, but it also seems possible that ΔF_λ vanishes or that new physics arises at higher ω_0 . In the limit $\omega_0 \rightarrow \infty$, the spin-Peierls model maps to a Heisenberg model with only AFM order, but for small interaction ranges $1/\omega_0$ in time, the retardation in \hat{H}_λ effectively generates longer-range spin interactions and also higher-order corrections [28,29]. Such a mapping to the frustrated J_1 - J_2 model successfully describes the physics of the 1D spin-Peierls model [30,31]. The complex phase diagrams of frustrated spin chains can also be found in electron-phonon models where ω_0 drives the competition between different $2k_F$ orders separated by a 1D DQCP [77]. On the honeycomb lattice, the J_1 - J_2 model has been studied on small clusters using exact diagonalization [78,79] and the density-matrix renormalization group [80–82]. As a function of increasing ratio J_2/J_1 , these studies found AFM, plaquette VBS, and staggered VBS order. The AFM-VBS transition was interpreted in terms of a DQCP [79–82], whereas an intermediate spin-liquid phase was also discussed [83]. Whether the physics of the J_1 - J_2 model appears at high ω_0 depends on two questions: (i) How do the effective nearest- and next-nearest-neighbor couplings $J_{1,2}(\omega_0, \lambda)$ depend on the parameters of the spin-Peierls model? In particular, will they reach a nontrivial regime in the phase diagram beyond AFM order? (ii) Do other operators become relevant in the mapping? The latter must be true for $\omega_0/J < 0.5$. Although VBS order appears in both models at $\mathbf{Q}_{\text{VBS}} = (2\pi/3, -2\pi/3)$, our results show columnar instead of plaquette order. Therefore, the adiabatic regime $\omega_0 \ll J$ is not described by the J_1 - J_2 model. While this is not surprising because the mapping should hold only at high ω_0 , the 1D problem is governed by the J_1 - J_2 model even at frequencies as low as $\omega_0/J = 0.25$ [27]. As there is only one possible VBS pattern in 1D, the nature of the VBS phase cannot change with ω_0 . Whether quantum lattice fluctuations can change the ground-state physics in 2D remains open.

Our results on the honeycomb lattice demonstrate that spin-phonon coupling can induce VBS order in a 2D antiferromagnet. Although a previous QMC study did not find a VBS phase on the square lattice [43], it is likely to exist in the regime $\lambda > 2$ not accessible to simulations. While spin-phonon interactions are a relevant mechanism in materials, the critical couplings found in this Letter are rather strong, as is also the case in many other spin models, e.g., the J - Q models [8]. A coupling to phonons was found to be important in combination with frustration [84], e.g., on hexagonal [85] or pyrochlore lattices [86,87]. Moreover, the spin-Peierls model is closely related to electron-phonon models: it corresponds

to a Su-Schrieffer-Heeger (SSH) model [88] with infinite Hubbard repulsion. Recently, determinantal QMC studies of the 2D SSH model with quantum phonons were carried out [89,90], but available system sizes were restricted by the difficult phonon sampling. On the square lattice, the SSH model supports VBS order at $\mathbf{Q}_{\text{VBS}} = (\pi, \pi)$ [90], whereas the influence of the Hubbard repulsion is still under debate [34,37]. On the honeycomb lattice, QMC results are available only for Holstein phonons which lead to a charge density wave phase [91–93]. Kekulé order was proposed to appear from a coupling to SSH phonons [94–96]. Recently, the SSH-Hubbard model was studied in the limit $\omega_0 \rightarrow \infty$, where a direct (DQCP) transition between columnar VBS and AFM order was reported [49], as well as a fermion-induced quantum critical point between a Dirac semimetal and VBS order [53]. Our results in the large- U limit suggest that Kekulé order and the corresponding transitions also exist at finite ω_0 but the AFM-VBS transition might turn first order for low ω_0 .

Conclusions and outlook. We demonstrated that VBS order can arise in a spin- $\frac{1}{2}$ Heisenberg model coupled to phonons. The first-order transition from AFM to columnar VBS order disagrees with the putative DQCP scenario on the honeycomb lattice but can be tuned towards weakly first order when quantum lattice fluctuations become stronger. Our results establish retardation effects as an important influence on the AFM-VBS transition that was not considered in previous studies. Our recently developed QMC method for retarded interactions [62] enables future work in this direction. In particular, it seems possible to engineer different orders via an appropriate coupling to phonons and thereby extend the zoo of models that show nontrivial phases in sign-problem-free QMC simulations. While retardation is an established mechanism to induce frustrated interactions in 1D models, the columnar VBS order at $\omega_0/J < 0.5$ is in contrast to the plaquette VBS order found in the J_1 - J_2 model [78–82]. It remains an open question whether the 2D spin-Peierls model displays the phases of the J_1 - J_2 model or any other nontrivial physics at higher ω_0 . Moreover, it will be of interest to explore how thermally generated phonon fluctuations modulate the exchange integral $J_{ij}(\hat{Q}_{ij})$ in the VBS phase and lead to a disordered phase. Finally, the possibility of finding Kekulé order in Dirac or spin systems motivates future studies of phonon coupling.

Acknowledgments. I thank F. Assaad, J. Freericks, M. Hohenadler, and F. Parisen Toldin for helpful discussions. This work was supported by the U.S. Department of Energy (DOE), Office of Science, Basic Energy Sciences (BES) under Award No. DE-FG02-08ER46542. The author gratefully acknowledges the Gauss Centre for Supercomputing e.V. [97] for funding this project by providing computing time on the GCS Supercomputer SuperMUC-NG at the Leibniz Supercomputing Centre [98] (Project No. pr53ju).

[1] S. Sachdev, Quantum magnetism and criticality, *Nat. Phys.* **4**, 173 (2008).

[2] N. Read and S. Sachdev, Valence-Bond and Spin-Peierls Ground States of Low-Dimensional Quantum Antiferromagnets, *Phys. Rev. Lett.* **62**, 1694 (1989).

[3] N. Read and S. Sachdev, Spin-Peierls, valence-bond solid, and Néel ground states of low-dimensional quantum antiferromagnets, *Phys. Rev. B* **42**, 4568 (1990).

[4] M. Levin and T. Senthil, Deconfined quantum criticality and Néel order via dimer disorder, *Phys. Rev. B* **70**, 220403(R) (2004).

- [5] T. Senthil, A. Vishwanath, L. Balents, S. Sachdev, and M. P. A. Fisher, Deconfined quantum critical points, *Science* **303**, 1490 (2004).
- [6] T. Senthil, L. Balents, S. Sachdev, A. Vishwanath, and M. P. A. Fisher, Quantum criticality beyond the Landau-Ginzburg-Wilson paradigm, *Phys. Rev. B* **70**, 144407 (2004).
- [7] I. Kimchi, A. Nahum, and T. Senthil, Valence Bonds in Random Quantum Magnets: Theory and Application to YbMgGaO_4 , *Phys. Rev. X* **8**, 031028 (2018).
- [8] A. W. Sandvik, Evidence for Deconfined Quantum Criticality in a Two-Dimensional Heisenberg Model with Four-Spin Interactions, *Phys. Rev. Lett.* **98**, 227202 (2007).
- [9] R. G. Melko and R. K. Kaul, Scaling in the Fan of an Unconventional Quantum Critical Point, *Phys. Rev. Lett.* **100**, 017203 (2008).
- [10] A. W. Sandvik, Continuous Quantum Phase Transition between an Antiferromagnet and a Valence-Bond Solid in Two Dimensions: Evidence for Logarithmic Corrections to Scaling, *Phys. Rev. Lett.* **104**, 177201 (2010).
- [11] F.-J. Jiang, M. Nyfeler, S. Chandrasekharan, and U.-J. Wiese, From an antiferromagnet to a valence bond solid: Evidence for a first-order phase transition, *J. Stat. Mech.* (2008) P02009.
- [12] A. B. Kuklov, M. Matsumoto, N. V. Prokof'ev, B. V. Svistunov, and M. Troyer, Deconfined Criticality: Generic First-Order Transition in the $\text{SU}(2)$ Symmetry Case, *Phys. Rev. Lett.* **101**, 050405 (2008).
- [13] B. Zhao, P. Weinberg, and A. W. Sandvik, Symmetry-enhanced discontinuous phase transition in a two-dimensional quantum magnet, *Nat. Phys.* **15**, 678 (2019).
- [14] J. W. Bray, H. R. Hart, L. V. Interrante, I. S. Jacobs, J. S. Kasper, G. D. Watkins, S. H. Wee, and J. C. Bonner, Observation of a Spin-Peierls Transition in a Heisenberg Antiferromagnetic Linear-Chain System, *Phys. Rev. Lett.* **35**, 744 (1975).
- [15] M. Hase, I. Terasaki, and K. Uchinokura, Observation of the Spin-Peierls Transition in Linear Cu^{2+} (Spin-1/2) Chains in an Inorganic Compound CuGeO_3 , *Phys. Rev. Lett.* **70**, 3651 (1993).
- [16] E. Pytte, Peierls instability in Heisenberg chains, *Phys. Rev. B* **10**, 4637 (1974).
- [17] M. C. Cross and D. S. Fisher, A new theory of the spin-Peierls transition with special relevance to the experiments on TTFCuBDT , *Phys. Rev. B* **19**, 402 (1979).
- [18] D. Augier and D. Poilblanc, Dynamical properties of low-dimensional and spin-Peierls systems, *Eur. Phys. J. B* **1**, 19 (1998).
- [19] D. Augier, D. Poilblanc, E. Sørensen, and I. Affleck, Dynamical effects of phonons on soliton binding in spin-Peierls systems, *Phys. Rev. B* **58**, 9110 (1998).
- [20] G. Wellein, H. Fehske, and A. P. Kampf, Peierls Dimerization with Nonadiabatic Spin-Phonon Coupling, *Phys. Rev. Lett.* **81**, 3956 (1998).
- [21] R. J. Bursill, R. H. McKenzie, and C. J. Hamer, Phase Diagram of a Heisenberg Spin-Peierls Model with Quantum Phonons, *Phys. Rev. Lett.* **83**, 408 (1999).
- [22] A. Weiße, G. Hager, A. R. Bishop, and H. Fehske, Phase diagram of the spin-Peierls chain with local coupling: Density-matrix renormalization-group calculations and unitary transformations, *Phys. Rev. B* **74**, 214426 (2006).
- [23] A. W. Sandvik, R. R. P. Singh, and D. K. Campbell, Quantum Monte Carlo in the interaction representation: Application to a spin-Peierls model, *Phys. Rev. B* **56**, 14510 (1997).
- [24] R. W. Kühne and U. Löw, Thermodynamical properties of a spin- $\frac{1}{2}$ Heisenberg chain coupled to phonons, *Phys. Rev. B* **60**, 12125 (1999).
- [25] A. W. Sandvik and D. K. Campbell, Spin-Peierls Transition in the Heisenberg Chain with Finite-Frequency Phonons, *Phys. Rev. Lett.* **83**, 195 (1999).
- [26] F. Michel and H.-G. Evertz, Lattice dynamics of the Heisenberg chain coupled to finite frequency bond phonons, *arXiv:0705.0799*.
- [27] H. Suwa and S. Todo, Generalized Moment Method for Gap Estimation and Quantum Monte Carlo Level Spectroscopy, *Phys. Rev. Lett.* **115**, 080601 (2015).
- [28] K. Kuboki and H. Fukuyama, Spin-Peierls transition with competing interactions, *J. Phys. Soc. Jpn.* **56**, 3126 (1987).
- [29] G. S. Uhrig, Nonadiabatic approach to spin-Peierls transitions via flow equations, *Phys. Rev. B* **57**, R14004 (1998).
- [30] A. Weiße, G. Wellein, and H. Fehske, Quantum lattice fluctuations in a frustrated Heisenberg spin-Peierls chain, *Phys. Rev. B* **60**, 6566 (1999).
- [31] C. Raas, U. Löw, G. S. Uhrig, and R. W. Kühne, Spin-phonon chains with bond coupling, *Phys. Rev. B* **65**, 144438 (2002).
- [32] S. Sachdev, *Quantum Phase Transitions*, 2nd ed. (Cambridge University Press, Cambridge, 2011).
- [33] F. C. Zhang and P. Prelovsek, Dimerization in the two-dimensional Hubbard model, *Phys. Rev. B* **37**, 1569 (1988).
- [34] S. Tang and J. E. Hirsch, Peierls instability in the two-dimensional half-filled Hubbard model, *Phys. Rev. B* **37**, 9546 (1988).
- [35] S. Mazumdar, Comment on Peierls instability in the two-dimensional half-filled Hubbard model, *Phys. Rev. B* **39**, 12324 (1989).
- [36] Q. Yuan and T. Kopp, Coexistence of the bond-order wave and antiferromagnetism in a two-dimensional half-filled Peierls-Hubbard model, *Phys. Rev. B* **65**, 085102 (2002).
- [37] J. Sirker, A. Klümper, and K. Hamacher, Ground-state properties of two-dimensional dimerized Heisenberg models, *Phys. Rev. B* **65**, 134409 (2002).
- [38] C. H. Aits, U. Löw, A. Klümper, and W. Weber, Structural and magnetic instabilities of two-dimensional quantum spin systems, *Phys. Rev. B* **74**, 014425 (2006).
- [39] S. Chiba, Y. Baba, and Y. Ono, Two-dimensional spin-Peierls state with a multimode lattice distortion, *J. Phys. Soc. Jpn.* **75**, 034705 (2006).
- [40] P. W. Anderson, The resonating valence bond state in La_2CuO_4 and superconductivity, *Science* **235**, 1196 (1987).
- [41] S. A. Kivelson, D. S. Rokhsar, and J. P. Sethna, Topology of the resonating valence-bond state: Solitons and high- T_c superconductivity, *Phys. Rev. B* **35**, 8865 (1987).
- [42] S. Mazumdar, Valence-bond approach to two-dimensional broken symmetries: Application to La_2CuO_4 , *Phys. Rev. B* **36**, 7190 (1987).
- [43] C. H. Aits and U. Löw, Thermodynamic properties of the two-dimensional $S = \frac{1}{2}$ Heisenberg antiferromagnet coupled to bond phonons, *Phys. Rev. B* **68**, 184416 (2003).

- [44] S. Pujari, K. Damle, and F. Alet, Néel-State to Valence-Bond-Solid Transition on the Honeycomb Lattice: Evidence for Deconfined Criticality, *Phys. Rev. Lett.* **111**, 087203 (2013).
- [45] M. S. Block, R. G. Melko, and R. K. Kaul, Fate of $\mathbb{C}\mathbb{P}^{N-1}$ Fixed Points with q Monopoles, *Phys. Rev. Lett.* **111**, 137202 (2013).
- [46] K. Harada, T. Suzuki, T. Okubo, H. Matsuo, J. Lou, H. Watanabe, S. Todo, and N. Kawashima, Possibility of deconfined criticality in $SU(N)$ Heisenberg models at small N , *Phys. Rev. B* **88**, 220408(R) (2013).
- [47] S. Pujari, F. Alet, and K. Damle, Transitions to valence-bond solid order in a honeycomb lattice antiferromagnet, *Phys. Rev. B* **91**, 104411 (2015).
- [48] T. Sato, M. Hohenadler, and F. F. Assaad, Dirac Fermions with Competing Orders: Non-Landau Transition with Emergent Symmetry, *Phys. Rev. Lett.* **119**, 197203 (2017).
- [49] Z.-X. Li, S.-K. Jian, and H. Yao, Deconfined quantum criticality and emergent $SO(5)$ symmetry in fermionic systems, [arXiv:1904.10975](https://arxiv.org/abs/1904.10975).
- [50] C.-Y. Hou, C. Chamon, and C. Mudry, Electron Fractionalization in Two-Dimensional Graphenelike Structures, *Phys. Rev. Lett.* **98**, 186809 (2007).
- [51] S. Ryu, C. Mudry, C.-Y. Hou, and C. Chamon, Masses in graphenelike two-dimensional electronic systems: Topological defects in order parameters and their fractional exchange statistics, *Phys. Rev. B* **80**, 205319 (2009).
- [52] B. Roy and I. F. Herbut, Unconventional superconductivity on honeycomb lattice: Theory of Kekulé order parameter, *Phys. Rev. B* **82**, 035429 (2010).
- [53] Z.-X. Li, Y.-F. Jiang, S.-K. Jian, and H. Yao, Fermion-induced quantum critical points, *Nat. Commun.* **8**, 314 (2017).
- [54] M. M. Scherer and I. F. Herbut, Gauge-field-assisted Kekulé quantum criticality, *Phys. Rev. B* **94**, 205136 (2016).
- [55] L. Classen, I. F. Herbut, and M. M. Scherer, Fluctuation-induced continuous transition and quantum criticality in Dirac semimetals, *Phys. Rev. B* **96**, 115132 (2017).
- [56] X. Y. Xu, K. T. Law, and P. A. Lee, Kekulé valence bond order in an extended Hubbard model on the honeycomb lattice with possible applications to twisted bilayer graphene, *Phys. Rev. B* **98**, 121406(R) (2018).
- [57] Y. Da Liao, Z. Y. Meng, and X. Y. Xu, Valence Bond Orders at Charge Neutrality in a Possible Two-Orbital Extended Hubbard Model for Twisted Bilayer Graphene, *Phys. Rev. Lett.* **123**, 157601 (2019).
- [58] B. Roy and V. Juričić, Fermionic multicriticality near Kekulé valence-bond ordering on a honeycomb lattice, *Phys. Rev. B* **99**, 241103(R) (2019).
- [59] K. K. Gomes, W. Mar, W. Ko, F. Guinea, and H. C. Manoharan, Designer Dirac fermions and topological phases in molecular graphene, *Nature (London)* **483**, 306 (2012).
- [60] C. Gutiérrez, C.-J. Kim, L. Brown, T. Schiros, D. Nordlund, E. B. Lochocki, K. M. Shen, J. Park, and A. N. Pasupathy, Imaging chiral symmetry breaking from Kekulé bond order in graphene, *Nat. Phys.* **12**, 950 (2016).
- [61] Y. Cao, V. Fatemi, S. Fang, K. Watanabe, T. Taniguchi, E. Kaxiras, and P. Jarillo-Herrero, Unconventional superconductivity in magic-angle graphene superlattices, *Nature (London)* **556**, 43 (2018).
- [62] M. Weber, F. F. Assaad, and M. Hohenadler, Directed-Loop Quantum Monte Carlo Method for Retarded Interactions, *Phys. Rev. Lett.* **119**, 097401 (2017).
- [63] A. W. Sandvik and J. Kurkijärvi, Quantum Monte Carlo simulation method for spin systems, *Phys. Rev. B* **43**, 5950 (1991).
- [64] O. F. Syljuåsen and A. W. Sandvik, Quantum Monte Carlo with directed loops, *Phys. Rev. E* **66**, 046701 (2002).
- [65] K. Hukushima and K. Nemoto, Exchange Monte Carlo Method and Application to Spin Glass Simulations, *J. Phys. Soc. Jpn.* **65**, 1604 (1996).
- [66] P. Sengupta, A. W. Sandvik, and D. K. Campbell, Bond-order-wave phase and quantum phase transitions in the one-dimensional extended Hubbard model, *Phys. Rev. B* **65**, 155113 (2002).
- [67] M. Weber, F. F. Assaad, and M. Hohenadler, Continuous-time quantum Monte Carlo for fermion-boson lattice models: Improved bosonic estimators and application to the Holstein model, *Phys. Rev. B* **94**, 245138 (2016).
- [68] M. Weber (unpublished).
- [69] K. Binder, Finite size scaling analysis of Ising model block distribution functions, *Z. Phys. B* **43**, 119 (1981).
- [70] See Supplemental Material at <http://link.aps.org/supplemental/10.1103/PhysRevB.103.L041105> for the data files for the results presented in this Letter.
- [71] K. Vollmayr, J. D. Reger, M. Scheucher, and K. Binder, Finite size effects at thermally-driven first order phase transitions: A phenomenological theory of the order parameter distribution, *Z. Phys. B* **91**, 113 (1993).
- [72] A. Schneider and H. Wierstorf, Gnuplot-colorbrewer: ColorBrewer color schemes for gnuplot (Version 1.0), Zenodo (2014), doi: [10.5281/zenodo.10282](https://doi.org/10.5281/zenodo.10282).
- [73] G. J. Sreejith and S. Powell, Scaling dimensions of higher-charge monopoles at deconfined critical points, *Phys. Rev. B* **92**, 184413 (2015).
- [74] Y. Nakayama and T. Ohtsuki, Necessary Condition for Emergent Symmetry from the Conformal Bootstrap, *Phys. Rev. Lett.* **117**, 131601 (2016).
- [75] M. A. Metlitski and R. Thormgren, Intrinsic and emergent anomalies at deconfined critical points, *Phys. Rev. B* **98**, 085140 (2018).
- [76] R. L. Frank and E. H. Lieb, Possible Lattice Distortions in the Hubbard Model for Graphene, *Phys. Rev. Lett.* **107**, 066801 (2011).
- [77] M. Weber, F. Parisen Toldin, and M. Hohenadler, Competing orders and unconventional criticality in the Su-Schrieffer-Heeger model, *Phys. Rev. Research* **2**, 023013 (2020).
- [78] H. Mosadeq, F. Shahbazi, and S. A. Jafari, Plaquette valence bond ordering in a J_1 - J_2 Heisenberg antiferromagnet on a honeycomb lattice, *J. Phys.: Condens. Matter* **23**, 226006 (2011).
- [79] A. F. Albuquerque, D. Schwandt, B. Hetényi, S. Capponi, M. Mambrini, and A. M. Läuchli, Phase diagram of a frustrated quantum antiferromagnet on the honeycomb lattice: Magnetic order versus valence-bond crystal formation, *Phys. Rev. B* **84**, 024406 (2011).
- [80] R. Ganesh, J. van den Brink, and S. Nishimoto, Deconfined Criticality in the Frustrated Heisenberg Honeycomb Antiferromagnet, *Phys. Rev. Lett.* **110**, 127203 (2013).
- [81] Z. Zhu, D. A. Huse, and S. R. White, Weak Plaquette Valence Bond Order in the $S=1/2$ Honeycomb J_1 - J_2 Heisenberg Model, *Phys. Rev. Lett.* **110**, 127205 (2013).

- [82] S.-S. Gong, D. N. Sheng, O. I. Motrunich, and M. P. A. Fisher, Phase diagram of the spin- $\frac{1}{2}$ J_1 - J_2 Heisenberg model on a honeycomb lattice, *Phys. Rev. B* **88**, 165138 (2013).
- [83] F. Ferrari, S. Bieri, and F. Becca, Competition between spin liquids and valence-bond order in the frustrated spin- $\frac{1}{2}$ Heisenberg model on the honeycomb lattice, *Phys. Rev. B* **96**, 104401 (2017).
- [84] F. Becca and F. Mila, Peierls-Like Transition Induced by Frustration in a Two-Dimensional Antiferromagnet, *Phys. Rev. Lett.* **89**, 037204 (2002).
- [85] X. Fabrèges, S. Petit, I. Mirebeau, S. Pailhès, L. Pinsard, A. Forget, M. T. Fernandez-Diaz, and F. Porcher, Spin-Lattice Coupling, Frustration, and Magnetic Order in Multiferroic RMnO_3 , *Phys. Rev. Lett.* **103**, 067204 (2009).
- [86] O. Tchernyshyov, R. Moessner, and S. L. Sondhi, Order by Distortion and String Modes in Pyrochlore Antiferromagnets, *Phys. Rev. Lett.* **88**, 067203 (2002).
- [87] K. Penc, N. Shannon, and H. Shiba, Half-Magnetization Plateau Stabilized by Structural Distortion in the Antiferromagnetic Heisenberg Model on a Pyrochlore Lattice, *Phys. Rev. Lett.* **93**, 197203 (2004).
- [88] W. P. Su, J. R. Schrieffer, and A. J. Heeger, Solitons in Polyacetylene, *Phys. Rev. Lett.* **42**, 1698 (1979).
- [89] S. Li and S. Johnston, Quantum Monte Carlo study of lattice polarons in the two-dimensional three-orbital Su-Schrieffer-Heeger model, *npj Quantum Mater.* **5**, 40 (2020).
- [90] B. Xing, W.-T. Chiu, D. Poletti, R. T. Scalettar, and G. G. Batrouni, Quantum Monte Carlo Simulations of the 2D Su-Schrieffer-Heeger Model, *Phys. Rev. Lett.* (to be published).
- [91] C. Chen, X. Y. Xu, Z. Y. Meng, and M. Hohenadler, Charge-Density-Wave Transitions of Dirac Fermions Coupled to Phonons, *Phys. Rev. Lett.* **122**, 077601 (2019).
- [92] Y.-X. Zhang, W.-T. Chiu, N. C. Costa, G. G. Batrouni, and R. T. Scalettar, Charge Order in the Holstein Model on a Honeycomb Lattice, *Phys. Rev. Lett.* **122**, 077602 (2019).
- [93] N. C. Costa, K. Seki, and S. Sorella, Magnetism and charge order in the honeycomb lattice, [arXiv:2009.05586](https://arxiv.org/abs/2009.05586).
- [94] K. Nomura, S. Ryu, and D.-H. Lee, Field-Induced Kosterlitz-Thouless Transition in the $N = 0$ Landau Level of Graphene, *Phys. Rev. Lett.* **103**, 216801 (2009).
- [95] M. Kharitonov, Phase diagram for the $\nu = 0$ quantum Hall state in monolayer graphene, *Phys. Rev. B* **85**, 155439 (2012).
- [96] L. Classen, M. M. Scherer, and C. Honerkamp, Instabilities on graphene's honeycomb lattice with electron-phonon interactions, *Phys. Rev. B* **90**, 035122 (2014).
- [97] www.gauss-centre.eu.
- [98] www.lrz.de.